Carbohydrate Polymers 90 (2012) 301–308

Contents lists available at SciVerse ScienceDirect

Carbohydrate Polymers

journal homepage: www.elsevier.com/locate/carbpol

Mechanical properties and *in vitro* degradation of electrospun bio-nanocomposite mats from PLA and cellulose nanocrystals

Qingfeng Shi[a,b,1], Chengjun Zhou[b,1], Yiying Yue[b], Weihong Guo[a], Yiqiang Wu[c], Qinglin Wu[b,*]

[a] School of Material Science & Engineering, East China University of Science & Technology, Shanghai 200237, China
[b] School of Renewable Natural Resource, Louisiana State University Agricultural Center, Baton Rouge, LA 70803, USA
[c] College of Material Science and Engineering, Central South University of Forestry and Technology, Changsha 410004, China

ARTICLE INFO

Article history:
Received 3 January 2012
Received in revised form 19 April 2012
Accepted 15 May 2012
Available online 23 May 2012

Keywords:
Electrospinning
Cellulose nanocrystals
Nanocomposites
Poly(lactic acid) (PLA)
In vitro degradation

ABSTRACT

Fibrous bio-nanocomposite mats consisting of cellulose nanocrystals (CNCs) and poly(lactic acid) (PLA) were electrospun from a solvent mixture consisting of N,N′-dimethylformamide and chloroform at room temperature. Morphological, mechanical and thermal properties, as well as *in vitro* degradation of nanocomposite mats were characterized as a function of material composition. Average diameter of the electrospun fibers decreased with increased CNC-loading level. Thermal stability, and tensile strength and modulus of nanocomposite mats were effectively improved by the addition of CNCs up to the 5 wt% level. The reinforcement of CNCs on electrospun mats was illustrated by the observation of SEM-based morphologies on the tensile fracturing process of nanocomposite mats. At the CNC content of 5 wt%, the maximum tensile stress and Young's modulus of the nanocomposite mats increased by 5 and 22 folds than those of neat PLA mats, respectively. Moreover, compared with neat PLA mats, the nanocomposite mats, especially at high CNC-loading levels, degraded more rapidly in phosphate-buffered saline solution.

1. Introduction

Poly(lactic acid) (PLA), a biodegradable polymer produced from renewable biomass resources, has been successfully electrospun to form micro or nanofibers for biomedical (*e.g.*, tissue engineering) and other related applications (Gupta, Revagade, & Hilborn, 2007; Yang, Murugan, Wang, & Ramakrishna, 2005). The scaffolds consisting of electrospun PLA fibers possessed desired porous structure and good biocompatibility (Kim et al., 2003). However, pure electrospun PLA fibers normally have weak mechanical properties and low thermal stability, which limit their application in many fields (Shi et al., 2011). Hence, enhancing mechanical properties of PLA fibers is desirable for biomedical applications, especially in engineered tissue scaffolds because that the materials has to meet controllable mechanical requirements for handling implant and supporting the process of tissue regeneration and structure degradation (Agarwal, Wendorff, & Greiner, 2009; Li, Laurencin, Caterson, Tuan, & Ko, 2002).

The most popular and effective methods for reinforcing PLA micro and/or nanofibers are modification of PLA matrix and the incorporation of nano-fillers (Chen, Shen, Chen, & Chen, 2010). Compounding PLA with fillers, especially with nano-scale fillers, could help improve composite mechanical properties. Noh, Lee, Shin, and Kim (2010) prepared nanofibers by PLA incorporated with bioactive glass nano-particulates using electrospinning. With the addition of 10 wt% nano-filler, the electrospun PLA/bioactive glass composites had greatly enhanced mechanical properties, excellent *in vitro* degradation and cell response properties. Recently, cellulose nanocrystals (CNCs) from microcrystalline cellulose (MCC) were used as reinforcement agents for PLA/cellulose nanocomposite fibers (Xiang, Joo, & Frey, 2009), which were electrospun at elevated temperatures using N,N′-dimethylformamide (DMF) solvent. The thermal stabilization of obtained nanocomposite mats was also improved.

The nontoxic and biodegradable CNCs are short crystalline rods in a length of micro to nanometers scale with an estimated Young's modulus of 138 GPa (Nishino, Takano, & Nakamae, 1995) and strength in the order of 7 GPa. It can be produced by chemical (acid or alkali) and physical treatments of biomass-based cellulose including plant, animal and bacteria (Eichhorn, 2011; Habibi, Lucia, & Rojas, 2010). In our recent study, CNCs from a combined acid hydrolysis and high pressure homogenization process of MCC and cotton were used to reinforce polyethylene oxide (PEO) (Zhou, Chu, Wu, & Wu, 2011) and polyacrylamide (PAM) (Zhou, Wu, Yue, & Zhang, 2011). In particular, it was found that the mechanical properties of electrospun PEO/CNC nanocomposite fibrous mats were markedly improved by using CNCs, which are well-dispersed in the

* Corresponding author. Tel.: +1 225 578 8369; fax: +1 225 578 4251.
E-mail address: wuqing@lsu.edu (Q. Wu).
[1] These authors contributed equally to this work.

0144-8617/$ – see front matter © 2012 Elsevier Ltd. All rights reserved.
http://dx.doi.org/10.1016/j.carbpol.2012.05.042

as-spun nanofibers. The reinforcement is benefited from smaller dimensions (especially in length) of CNCs, which were processed by high pressure homogenization (Habibi et al., 2010), producing strong mechanical shearing to effectively split natural fibers (Zhou & Wu, 2011).

In this study, CNCs originated from the combined acid hydrolysis and high pressure homogenization of cotton was incorporated into PLA fibers to improve the mechanical properties of PLA/CNC nanocomposite mats. PLA/CNC nanocomposite mats were electrospun at room temperature by using a solvent mixture including chloroform with low boiling point and DMF. Although many papers have reported electrospun polymer nanofibers reinforced with CNCs even including a few studies concerning PLA systems (Ramirez, 2010; Xiang et al., 2009), the hydrolytic degradation behavior has not yet been investigated. Considering the excellent biodegradation of CNCs, exploring the degradation of fully bio-based PLA/CNC composite nanofibers will be highly beneficial to their development in biomedicine fields. The objectives of the present study were to investigate *in vitro* degradation in phosphate buffer solution (PBS), morphology, thermal and mechanical properties of electrospun PLA/CNC bio-nanocomposite nanofibrous mats for their potential application in the tissue engineering scaffold. Moreover, the present work also illustrated systematically the reinforce mechanism of CNCs on electrospun PLA/CNC bio-nanocomposite nanofibrous mats by studying the tensile behavior of mats and by comparing the difference between electrospun mats and cast films.

2. Experimental

2.1. Materials

CNCs originated from cotton fabrics (provided by the USDA ARS Southern Regional Research Center in New Orleans, LA, United States) were prepared by a combined process of acid hydrolysis with 64% H_2SO_4 and high-pressure homogenization according to our previous report (Yue, 2011; Zhou, Wu, et al., 2011). The obtained CNCs had length ranging from 40 to 120 nm and an average diameter of 8.7 ± 1.7 nm based on the observation of Transmission electron microscopy (TEM). The CNC aqueous suspension was freeze-dried to obtain dry CNC material for the current work. Semi-crystalline grade PLA (4032D, melting-flow index of 1.64 g min^{-1}, M_w = 100,000) was supplied by Nature Works Inc. (Minnetonka, MN, United States). It was dried in a vacuum oven at 60 °C for 24 h prior to use. DMF and chloroform were purchased from Sigma–Aldrich Inc. (St. Louis, MO, United States). All reagents were used without further purification.

2.2. Fabrication of electrospun mats and cast films

PLA pellet and freeze-dried CNC powder were added to the mixture of solvents chloroform/DMF (4/1, v/v). The mixture was stirred and heated for 30 min at 65 °C to fully dissolve PLA. It was then transferred to an ultrasonic bath for 30 min until the well dispersion of CNCs. The final concentration of PLA in the mixture was 15 wt%. The compositions of CNCs were 0, 1, 2, 5, and 10 wt% based on the weight of PLA.

The obtained suspensions were loaded in a 1-ml plastic syringe with a stainless steel needle (internal diameter = 0.584 mm). The needle was connected to a high voltage power supply (Gamma High Voltage Research, Ormond Beach, FL, United States), which generated a positive DC voltage of 15 kV. The flow rate of the suspension was controlled at 1.5 ml h^{-1} by a Chemyx Fusion 100 syringe pump (Chemyx Inc., Stafford, TX, United States). A piece of grounded aluminum foil used as collector was placed under the capillary needle tip with a distance of 20 cm. The obtained fibers were collected as mats, which were vacuum-dried at 80 °C for 24 h and then stored in a desiccator prior to characterization. All mats were prepared using 1 ml of the electrospinning solution or suspension and exactly same electrospinning parameters to ensure that the changes in microstructures and properties of mats were originated from the incorporation of CNCs as much as possible.

PLA/CNC suspensions were also cast onto clean glass plates and dried in open air at room temperature to form cast films with a 15 μm thickness for comparison with the electrospun mats. The obtained films were vacuum-dried at 80 °C for 24 h.

2.3. Measurement and characterization

2.3.1. Electrospinning suspension

Electrical conductivity of the prepared electrospinning suspensions were determined at room temperature using a Jenway Model 4330 conductivity and PH meter (Bath, United Kingdom). The viscosity of the suspensions were measured by a AR2000 rheometer (TA Instruments, New Castle, DE, United States) at 25 °C and the shear rate was fixed at 10 s^{-1}.

2.3.2. Morphological observation

The surfaces of the samples from the electrospun mats were sputter-coated with a thin layer of gold and their morphologies were evaluated with a Hitachi S-3600N scanning electron microscope (SEM, Hitachi High Technologies America, Schaumburg, IL, United States) at 25.0 kV. The fiber diameters were obtained from the analysis of SEM images using Adobe Photoshop, with 20 nanofibers randomly selected from each image.

2.3.3. Thermal analysis

Thermogravimetric analysis (TGA) was conducted using a TA Q50 analyzer (TA Instruments, New Castle, DE, United States) to study thermal decomposition of electrospun PLA and PLA/CNC fibrous mats. Samples of 5–10 mg were heated from room temperature to 600 °C at a rate of 10 °C min^{-1} in a N_2 atmosphere. The weight-loss rate was obtained from derivative thermogravimetric (DTG) data. The onset degradation temperature (T_{onset}) was defined as the intersection temperature of tangents drawn from the TG curves.

Differential scanning calorimetry (DSC) measurements of the electrospun PLA and PLA/CNC mats were performed with a TA Q100 system. To remove any thermal history, samples of 5–10 mg were heated to 200 °C at a heating rate of 30 °C min^{-1}, and maintained at this temperature for 5 min followed by cooling to room temperature at a rate of 10 °C min^{-1}. During subsequent test runs, the samples were reheated to 200 °C at a heating rate of 10 °C min^{-1} and test data collected.

The crystallinity of the samples was calculated using the following equation:

$$X_c = \frac{\Delta H_m - \Delta H_{cc}}{\Delta H_{m0}} \times 100\% \quad (1)$$

where X_c (%) is the crystallinity, ΔH_m (J/g) is the heat of fusion from the second heating circle, ΔH_{cc} (J/g) is the heat of cold crystallization, and ΔH_{m0} is the heat of fusion for 100% crystalline PLA, taken as 93 J/g (Mihai, Huneault, Favis, & Li, 2007). The absolute crystallinity of PLA in the composites was calculated as X_p:

$$X_p = \frac{X_c}{w} \quad (2)$$

where w is the weight fraction of PLA in the composites.

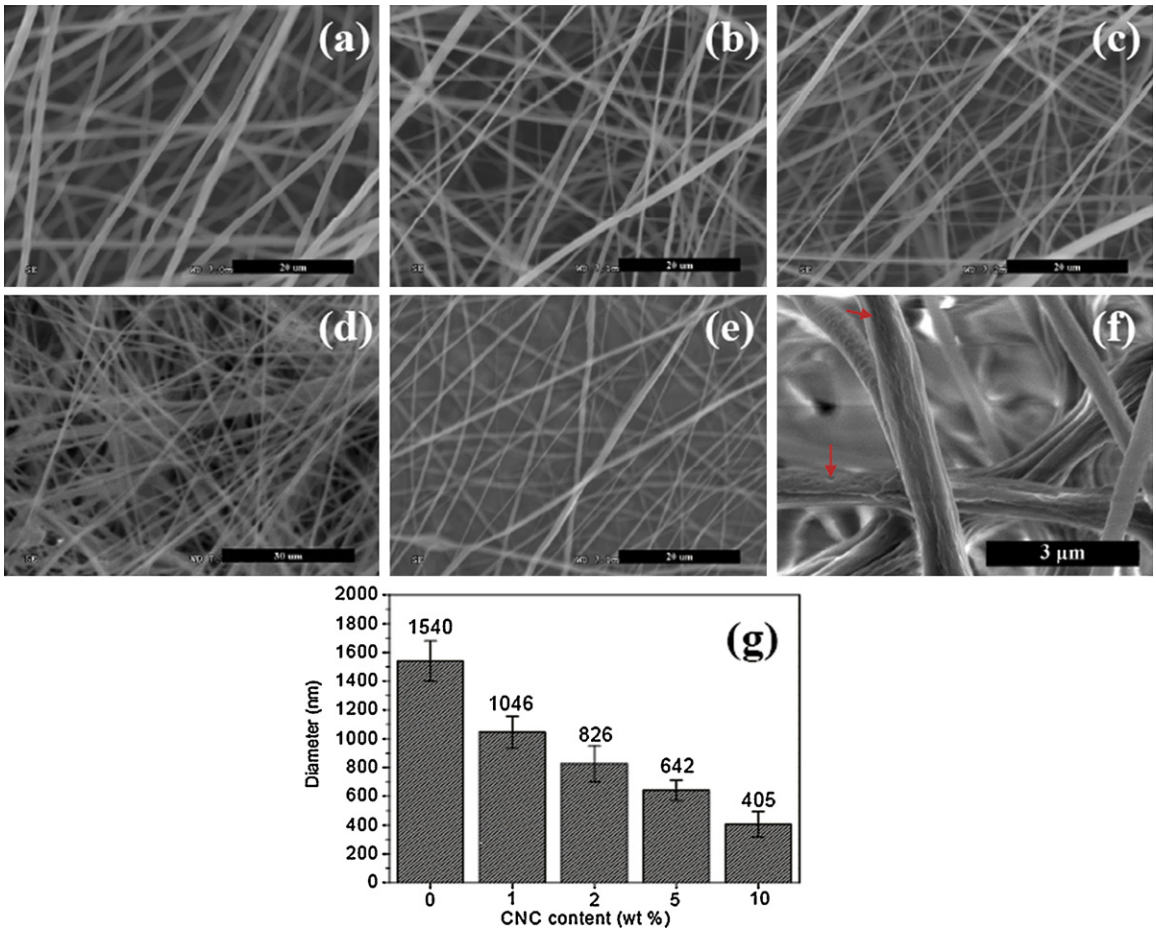

Fig. 1. SEM micrographs of the electrospun fibrous mats: (a) neat PLA, (b) PLA/1 wt% CNC, (c) PLA/2 wt% CNC, (d) PLA/5 wt% CNC, (e) PLA/10 wt% CNC, and (f) PLA/5 wt% CNC with higher magnification; and (g) the relationship between CNC content and the diameter distribution for PLA/CNC fibers.

2.3.4. Mechanical property analysis

Tensile strength and elongation at break were measured using the TA AR2000 rheometer with a solid fixture. Mats were carefully peeled off from the surface of aluminum foil and then placed between two pieces of weighing paper to avoid any direct touch damage on the mat surfaces during sample preparation. The tensile gauge length was 10 mm. The speed of tensile testing was 10 μm/s and three specimens with dimension of 20 mm in length, 3 mm in width, and 45 ± 6 μm in thickness were used for each sample group. The stress and strain were calculated through the machine-recorded force and displacement based on the initial cross-section area and gauge length, respectively. The Young's modulus was calculated through the linear regression analysis of the initial linear portion of the stress–strain curves.

2.3.5. In vitro degradation

The dried electrospun samples were cut into square pieces of 15 mm and weighed. They were placed in sealed bottles containing 25 ml of PBS (PH = 7.3, Sigma–Aldrich Company). The bottles were immersed in a 37 °C water bath for one month. At target intervals, the samples were took out and washed in DI water, dried in a vacuum oven, and re-weighed.

3. Results and discussion

3.1. Morphologies of fibrous mats

SEM photographs of electrospun neat PLA and PLA/CNC fibrous mats are shown in Fig. 1. All fibers produced were homogeneous without visible beads, and exhibited the sharply decreased diameters with increased CNC content. Xiang et al. (2009) reported similar observations on the electrospun PLA/cellulose nanocomposite fibers. The calculated average diameters and diameter deviations of as-spun fibers are displayed in Fig. 1g. As shown, the average diameters of the as-spun neat PLA fibers and the PLA nanocomposite fibers with 1 wt% CNC-loading level were about 1.5 and 1 μm, respectively. The fiber diameters further decreased to 642 and 405 nm at 5 and 10 wt% CNC-loading levels, respectively. The distribution of fiber diameter was more uniform in the PLA/5 wt% CNC composite fibers compared with those of PLA/10 wt% CNC composite fibers. This was likely due to that the significant aggregation of CNCs occurred in the PLA/10 wt% CNC composite fibers, which obstructed the spinneret head and thus caused discontinuous fiber deposition during the electrospinning process. Fig. 1f shows surface microstructure of PLA/5 wt% CNC fibers with high magnification, on which there were many pores, as indicated by red arrows. This phenomena is similar to the previous report on electrospun PLA/CNC nanocomposite fibers (Ramirez, 2010). In general, there are two explanations for pore formation in electrospun fibers (*i.e.*, the exothermic reaction in the fibers and the rapid volatilization of solvent during the electrospinning process). For fibers produced in this study, the pore formation in PLA/CNC bio-nanocomposite fibers is more likely related to the volatilization of the solvents. Additionally, the phase separation between immiscible PLA and CNCs may induces the formation of pores (Casper, Stephens, Tassi, Chase, & Rabolt, 2004).

Generally, the change of diameter of electrospun nanofibers incorporated by nanoparticles was mostly attributed to the charge

Table 1
Viscosity and electrical conductivity of electrospinning PLA solution and PLA/CNC suspensions.

Sample[a]	Viscosity (mPa s)	Electrical conductivity ($\mu s\,cm^{-1}$)
PLA	14.5	0.45
PLA/1 wt% CNC	14.7	0.60
PLA/2 wt% CNC	15.1	0.62
PLA/5 wt% CNC	16.0	0.67
PLA/10 wt% CNC	16.2	0.66

[a] PLA concentration in the solution before adding CNCs was fixed at the 15 wt%. Target CNC amount was based on the weight of PLA in the formed solution. CNC were added to the 15 wt% of PLA solution to form the spinning suspensions.

density and visco-elastic behavior of electrospinning solutions (Greiner & Wendorff, 2007). As shown in Table 1, there were two important parameters of the electrospinning suspensions (*i.e.*, electrical conductivity and viscosity). Compared with neat PLA solution, the viscosity of the PLA/CNC suspensions increased slightly, while their electrical conductivity significantly increased because of the CNC surface having uronic acid and sulfate ester groups (Zhou, Wu, & Zhang, 2011; Zhou, Wang, & Wu, 2012). With increased CNC contents, there was a substantial increase in electrical conductivity for electrospinning suspensions. Increasing electrical conductivity for electrospinning solution or suspensions could result in a higher charge density on the surface of ejected jet during spinning, and then promote the formation of higher elongation forces to drive the jet under the electrical field (Zong et al., 2002). The enhanced electrostatic forces facilitate the jet to split in smaller and more spindle-like. Hence, the diameter of fibers formed becomes substantially smaller with increased CNC contents.

3.2. Thermal properties

TG and differential TG (DTG) curves of neat PLA and PLA/CNC mats are shown in Fig. 2a and b, respectively. Thermal parameters including T_{onset} and the maximum thermal degradation temperature (T_{max}) are summarized in Table 2. T_{onset} of neat PLA was 292 °C, while PLA/CNC nanocomposite mats, with the exception of the PLA/1 wt% CNC, had T_{onset} of greater than 300 °C. T_{max} of PLA/CNC mats also displayed a similar trend. The PLA/5 wt% CNC nanocomposite mats had the highest T_{onset} and T_{max} values, indicating that they had an improved heat resistance. Fig. 2a also reveals that the char yield of electrospun PLA/CNC nanocomposite mats increased with increased CNC content. The char yield is directly correlated to the potency of flame retardation for the composites (Vankrevelen, 1975). Increased char formation can limit the production of combustible gases, decrease the exothermicity of the pyrolysis reaction, and inhibit the thermal conductivity of the burning materials (Liepins & Pearce, 1976). Moreover, the increased crystallinity (discussed below with DSC data) could also improve the T_{max} of the composites (Kumar, Depan, Tomer, & Singh, 2009). Therefore, the increase of T_{max} of PLA/CNC nanocomposite mats was mostly attributed to the char formation and increased crystallinity in nanocomposites.

Fig. 2c (DSC curves) and Table 2 show that the cold crystallization temperature of PLA/CNC nanocomposite mats initially decreased, and then increased with increased CNC contents. It is likely attributed to that CNC promoted the cold crystallization at lower temperatures, while the aggregates of CNCs occurred at high loading levels were less effective in promoting crystallization due to decreased contact area between CNCs and PLA matrix. Moreover, at the high CNC contents, there were two melt peaks in the DSC

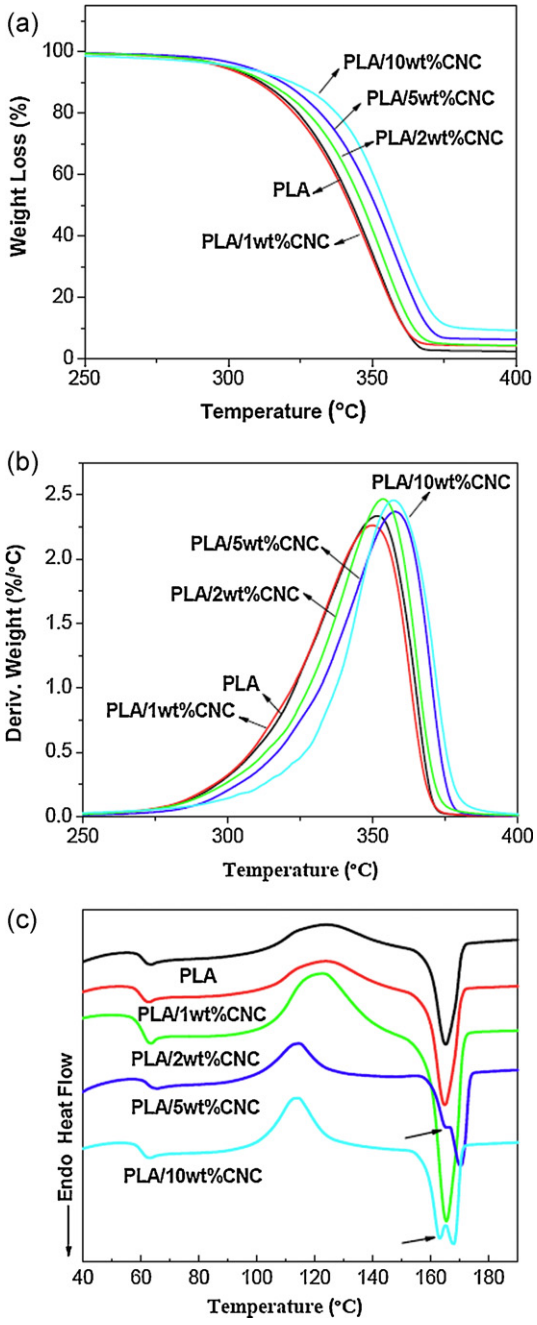

Fig. 2. TG (a), DTG (b) and DSC curves (c) of the electrospun neat PLA and PLA/CNC mats.

Table 2
Summary of TGA and DSC curves of electrospun PLA/CNC composite fibrous mats.

Sample	T_{onset} (°C)	T_{max} (°C)	T_g (°C)	T_{cc} (°C)	T_m (°C)	ΔH_m (J/g)	ΔH_{cc} (J/g)	X_c (%)	X_p (%)
PLA	292.2	351.8	60.4	123.3	165.1	35.2	35.3	0	0
PLA/1 wt% CNC	280.5	350.6	60.4	123.9	164.7	38.6	37.8	0.8	1.0
PLA/2 wt% CNC	304.4	353.1	60.2	122.6	165.3	34.9	32.6	2.5	2.6
PLA/5 wt% CNC	308.6	357.5	62.5	110.9	166.7	30.3	24.0	6.8	7.1
PLA/10 wt% CNC	305.4	356.4	60.5	113.8	163.1	26.5	23.8	3	3.3

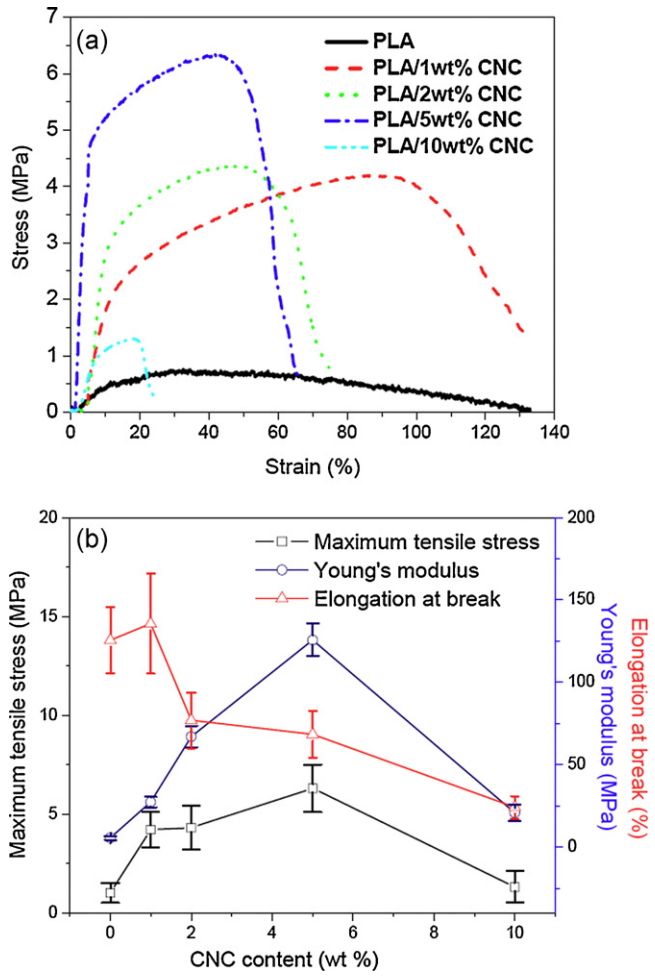

Fig. 3. Typical stress–strain curves of electrospun neat PLA and PLA/CNC mats (a), and tensile properties of electrospun PLA/CNC nanocomposite mats as a function of CNC content (b).

curves, suggesting that increased CNC contents promoted the rearrangement of PLA segments and the formation of heterogeneous crystal phases in PLA during thermal crystallization. The area of the lower melting temperature also increased with increased CNC contents from 5 to 10 wt%, indicating the formation of smaller and less dense crystals in the PLA matrix (Shi, Mou, Gao, Yang, & Guo, 2010).

As shown in Table 2, with increased CNC contents, the change of the glass transition temperature (T_g) of PLA nanocomposite mats was not obvious except T_g of PLA/5 wt% CNC mats being higher. It is likely because that the size PLA crystal phases were gradually restricted with increased CNC loading level up to 5 wt% and the aggregations of CNCs with 10 wt% loading weakened this impact because of reduced CNC/matrix interactions. Table 2 also shows that the crystallinity X_p of PLA increased with increased CNC content up to 5 wt%, which indicates that a low amount of CNCs could act as nucleating agents for improving the crystallization of PLA molecular chains.

3.3. Mechanical properties

Typical stress–strain curves of neat PLA and PLA nanocomposite mats are presented in Fig. 3a, and their maximum tensile stress (σ_{max}), Young's modulus (E), and the elongation at break (ε_b) are summarized in Fig. 3b. With increased CNC contents, σ_{max} and E of electrospun PLA/CNC nanocomposite mats had a marked improvement at the low CNC content levels, making mats stiffer and stronger. Compared with the neat electrospun PLA mats, the values of σ_{max} and E of PLA/5 wt% CNC nanocomposite mats increased by approximate 5 and 22 folds (6.3 and 125.6 MPa), respectively. However, at the10 wt% CNC content level, the tensile properties of PLA nanocomposite mats decreased sharply. It was likely attributed to the aggregation of CNCs at high loading levels in electrospun fibers, especially on the fiber surface (Xiang et al., 2009), which decreased crystallinity of PLA (Table 2) and weakened the cohesion between fibers. Furthermore, with increased CNC content, ε_b of PLA/CNC nanocomposite mats decreased gradually, making mats more resistant to deformation (Lee et al., 2008).

Due to the fact that the electrospun mats are non-woven fabrics, their mechanical properties are influenced by several factors including composition and structure of individual fibers and the interaction between fibers. In order to illustrate the reinforcement effect of CNCs on electrospun mats, the tensile behavior of electrospun PLA/5 wt% CNC nanocomposite mats was compared with that of the cast PLA/5 wt% CNC nanocomposite films. As shown in Fig. 4a, the cast PLA/5 wt% CNC nanocomposite films had a greater tensile strength and shorter elongation compared with these of electrospun PLA/5 wt% CNC nanocomposite mats because that the electrospun mats possessed low molecular chain orientation of non-aligned fibers (Ayutsede et al., 2006) and high porosity. There was also an obvious yield point during the tensile fracturing process for the cast films, which is similar as the regular tensile fracturing of polymer materials. Fig. 4b shows a scheme of tensile fracturing process of the cast films. At the beginning, the polymer chain segments in the cast films hardly moved, which represented the linear elastic stage. After a certain degree of segment movement (*i.e.*, beyond the yield point), polymer chains could not revert back to their original positions and the cast films reached plastic strain stage. After that, the crazes or defects might occur, and cause the rupture of the cast film in a short time to influence the tensile properties of the whole cast film. The existence of stiffer and stronger CNCs could improve the tensile modulus and strength of the cast nanocomposite films. There was a significant difference between electrospun mats and cast films in the tensile fracturing behavior, as shown in Fig. 4a. With increased strain, the tensile stress of electrospun mats increased sharply at the beginning, and then increased slowly over a relatively long period of strain followed by the final rupture, similar to other unaligned electrospun mats (Gomez-Tejedor, Van Overberghe, Rico, & Ribelles, 2011). Fig. 4c shows a scheme of the tensile fracturing of electrospun mats based on SEM photographs. At the beginning of tensile process, the mats were stretched in macroscopic view and most fibers in mats hardly moved attributed to the cohesion between fibers, which determined modulus of mats. When most fibers in mats reached the tightened form, yield of mats appeared, at which the interaction points among fibers were broken. With further increase of tensile strain, the fibers in mats were drawn out to highly align along the tensile direction. At this stage, single fiber has the same tensile behavior as the cast films as mentioned above. However, the rupture of individual fibers one by one did not influence the tensile properties of the whole mats, resulting in larger elongation at break for electrospun mats compared with the cast films. At the maximum tensile stress level, most fibers were necked and broken, leading to the final rupture of mats.

According to the above-mentioned analysis, the improvement in modulus of PLA/CNC nanocomposite mats mostly was ascribed to the enhanced interaction among fibers originated from more uniform and finer fibers by the incorporation of CNCs (Casper et al., 2004; Xiang et al., 2009), as shown in Fig. 1. While the impressive increase in the strength of PLA/CNC nanocomposite mats was mainly attributed to the addition of CNCs into PLA, which caused the increased crystallinity for PLA (Table 2) and the reduced loading

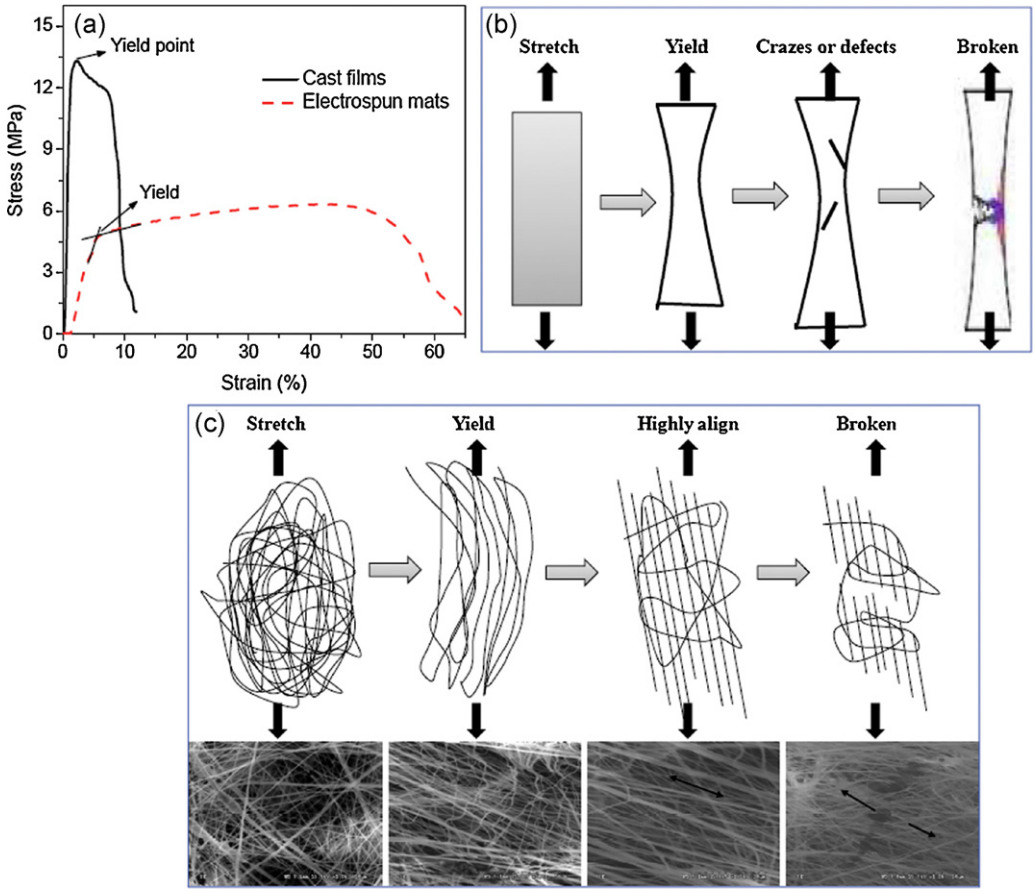

Fig. 4. Typical stress–strain curves of cast films and electrospun mats based on PLA/5 wt% CNC nanocomposite (a), scheme of tensile fracturing process of the cast films (b), and scheme and SEM-based morphologies of fracturing process of the electrospun mats (c).

force on PLA through the stress transfer from PLA to CNCs (Zhou, Chu, et al., 2011).

3.4. *In vitro* degradation

In vitro degradation of mats was evaluated by weight loss immerged into the PBS medium for one month. Fig. 5 shows the weight loss of mats as a function of the degradation time. As shown, all mats had a rapid degradation rate during the first several days. This was likely a result of the fast penetration of solvent into the spaces between fibers of highly porous mats to cause the simple hydrolysis on the easily accessible surfaces and phase interfaces followed by further degradation requiring long exposures for solvent to penetrate the denser phase (Vieira et al., 2011). After one month exposure, the weight loss of mats reached 14.7 wt% for neat PLA, 19.0 wt% for PLA/1 wt% CNC, 42.9 wt% for PLA/5 wt% CNC, and 38.9 wt% for PLA/10 wt% CNC, respectively. This result suggested that the *in vitro* degradability of PLA/CNC nanocomposite mats was higher than that of neat PLA mats likely because of the lower fiber diameter resulting in higher surface area for nanocomposite mats (You, Min, Lee, Lee, & Park, 2005). In addition, the result of Fig. 1 above exhibited a large number of well-defined pores occurred in the surface of PLA/CNC nanocomposite fibers, which is also probably responsible for more rapid degradation rates of PLA/CNC nanocomposite mats.

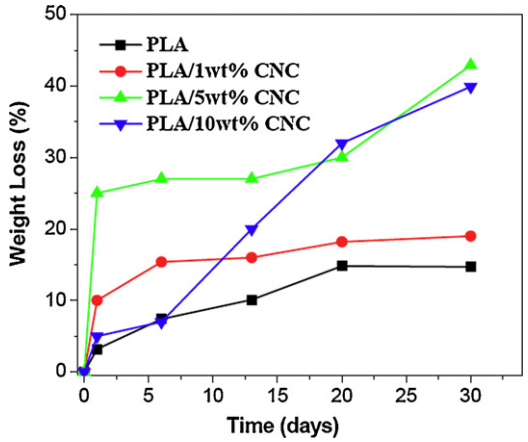

Fig. 5. Weight loss of electrospun neat PLA and PLA/CNC mats as a function of degradation time.

The SEM photographs in Fig. 6a and b show the morphologies of the neat PLA and PLA/5 wt% CNC mats with *in vitro* degradation after one month. The diameters of degraded fibers in nanocomposite mats were much larger than those in PLA mats, which supported the higher degradation ability in nanocomposite mats than PLA mats as shown in Fig. 5. From Fig. 6a and b, it also can be seen that there were several degraded phenomena in degradation processing including the hydrolysis, merged areas formed, ruptured fibers (pointed by the arrows in the insert of Fig. 6a), and possible bacterium degradation (pointed by the arrows in the insert of Fig. 6b), which promoted the degradation of mats.

It would be possible to recycle reinforced PLA nanocomposite mats and a pathway is shown in Fig. 6c. The first step of the *in vitro* degradation was swelling and hydrolysis, leading to rupturing of fibers. The second step was the eroding and more complete

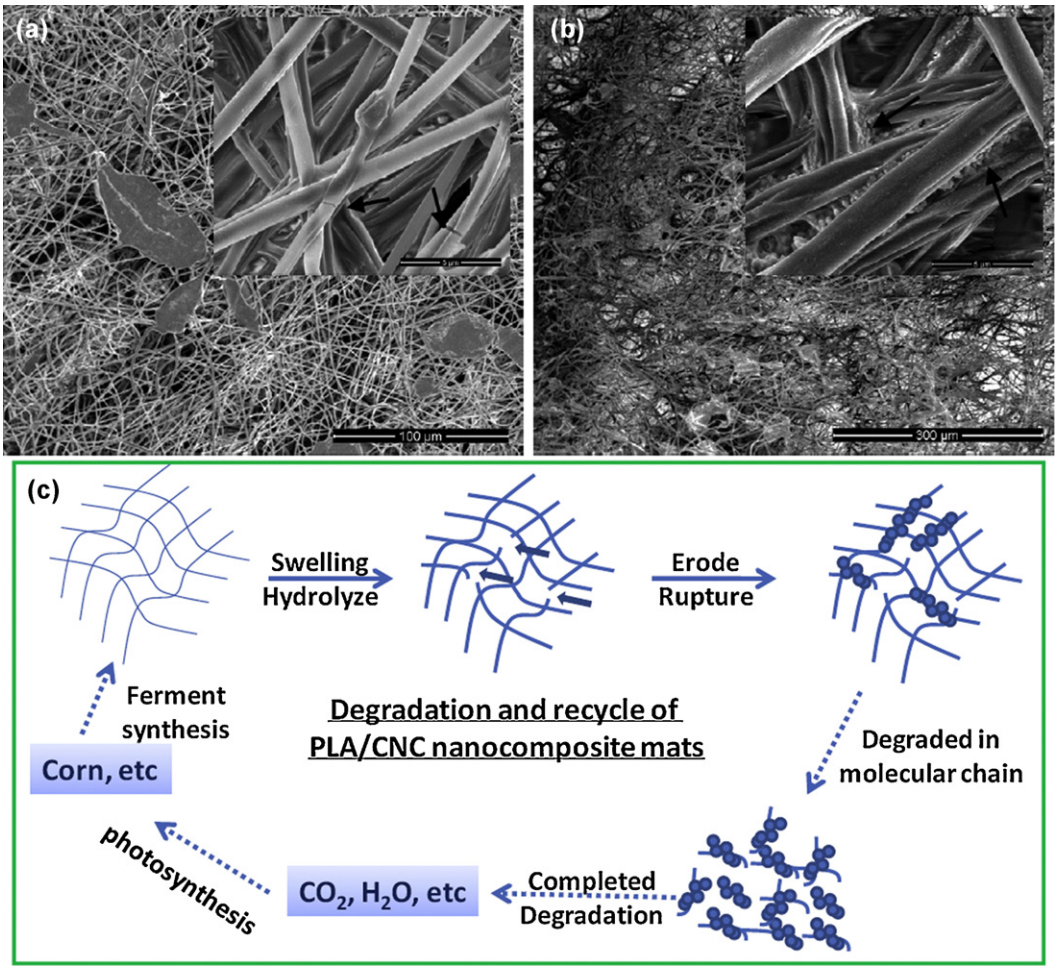

Fig. 6. SEM micrographs of *in vitro* degradation for neat PLA mats (a) and PLA/5 wt% CNC nanocomposite mats (b) after one month (the inserts showing enlarged SEM images), and (c) schematic diagram of possible *in vitro* degradation cycle in PLA/CNC nanocomposite mats.

degradation of fibers due to the uptake of PBS buffer. The aggregation and erosion of fibers in mats also occurred. In the final step, the polymer molecular chains would seriously degrade, followed by transformation to water and carbon dioxide after the enough *in vitro* degradation time. It might be a recyclable, green, and eco-friend process to produce fully biodegradable PLA/CNC nanocomposite mats.

4. Conclusions

Electrospun PLA/CNC nanocomposite mats were successfully prepared using chloroform/DMF mixture as solvent. With increased CNC content, the average fiber diameter of PLA/CNC fibers decreased sharply. The tensile results revealed that PLA nanocomposite mats had excellent mechanical properties at lower CNC content levels, especially at the 5 wt% CNC-loading level. Compared with the neat electrospun PLA mats, the maximum tensile stress and Young's modulus of PLA/CNC nanocomposite mats with a CNC content of 5 wt% increased by about 5 and 22 folds (*i.e.*, 6.3 and 125.6 MPa), respectively. The observation of SEM-based morphologies on the tensile fracturing process of nanocomposite mats illustrated that the improvement of strength and modulus was mostly ascribed to the reinforcement of CNCs, increased crystallinity of matrix, and more uniform and finer dimension of fibers. The incorporation of CNCs also enhanced the thermal stability and *in vitro* degradation rates of PLA/CNC nanocomposite mats. A possible degradation process in nanocomposite mats was proposed. This study demonstrated for the first time that bio-nanocomposite mats electrospun from PLA and CNCs mats had rapid *in vitro* biodegradability combined by impressive mechanical properties (especially in modulus), and are therefore particularly suitable for short-term applications in the tissue engineering scaffold and other fields.

Acknowledgments

This work is financially supported by the USDA Rural Development Biomass Initiative Program (68-3A75-6-508), National Key Technology R&D Program of China (2008BAC46B10), and 2010 start-up fund of Engineering Research Center of Biomass Materials, Ministry of Education, Southwest University of Science and Technology, Mianyang, China.

References

Agarwal, S., Wendorff, J. H., & Greiner, A. (2009). Progress in the field of electrospinning for tissue engineering applications. *Advanced Materials*, *21*(32–33), 3343–3351.

Ayutsede, J., Gandhi, M., Sukigara, S., Ye, H. H., Hsu, C. M., Gogotsi, Y., et al. (2006). Carbon nanotube reinforced Bombyx mori silk nanofibers by the electrospinning process. *Biomacromolecules*, *7*(1), 208–214.

Casper, C. L., Stephens, J. S., Tassi, N. G., Chase, D. B., & Rabolt, J. F. (2004). Controlling surface morphology of electrospun polystyrene fibers: Effect of humidity and molecular weight in the electrospinning process. *Macromolecules*, *37*(2), 573–578.

Chen, B. K., Shen, C. H., Chen, S. C., & Chen, A. F. (2010). Ductile PLA modified with methacryloyloxyalkyl isocyanate improves mechanical properties. *Polymer*, *51*(21), 4667–4672.

Eichhorn, S. J. (2011). Cellulose nanowhiskers: Promising materials for advanced applications. *Soft Matter*, *7*(2), 303–315.
Gomez-Tejedor, J. A., Van Overberghe, N., Rico, P., & Ribelles, J. L. G. (2011). Assessment of the parameters influencing the fiber characteristics of electrospun poly(ethyl methacrylate) membranes. *European Polymer Journal*, *47*(2), 119–129.
Greiner, A., & Wendorff, J. H. (2007). Electrospinning: A fascinating method for the preparation of ultrathin fibres. *Angewandte Chemie-International Edition*, *46*(30), 5670–5703.
Gupta, B., Revagade, N., & Hilborn, J. (2007). Poly(lactic acid) fiber: An overview. *Progress in Polymer Science*, *32*(4), 455–482.
Habibi, Y., Lucia, L. A., & Rojas, O. J. (2010). Cellulose nanocrystals: Chemistry, self-assembly, and applications. *Chemical Reviews*, *110*(6), 3479–3500.
Kim, K., Yu, M., Zong, X. H., Chiu, J., Fang, D. F., Seo, Y. S., et al. (2003). Control of degradation rate and hydrophilicity in electrospun non-woven poly(D,L-lactide) nanofiber scaffolds for biomedical applications. *Biomaterials*, *24*(27), 4977–4985.
Kumar, A. P., Depan, D., Tomer, N. S., & Singh, R. P. (2009). Nanoscale particles for polymer degradation and stabilization-Trends and future perspectives. *Progress in Polymer Science*, *34*(6), 479–515.
Lee, J., Tae, G., Kim, Y. H., Park, I. S., Kim, S. H., & Kim, S. H. (2008). The effect of gelatin incorporation into electrospun poly(L-lactide-co-epsilon-caprolactone) fibers on mechanical properties and cytocompatibility. *Biomaterials*, *29*(12), 1872–1879.
Li, W. J., Laurencin, C. T., Caterson, E. J., Tuan, R. S., & Ko, F. K. (2002). Electrospun nanofibrous structure: A novel scaffold for tissue engineering. *Journal of Biomedical Materials Research*, *60*(4), 613–621.
Liepins, R., & Pearce, E. M. (1976). Chemistry and toxicity of flame retardants for plastics. *Environmental Health Perspectives*, *17*(October), 55L 63.
Mihai, M., Huneault, M. A., Favis, B. D., & Li, H. B. (2007). Extrusion foaming of semi-crystalline PLA and PLA/thermoplastic starch blends. *Macromolecular Bioscience*, *7*(7), 907–920.
Nishino, T., Takano, K., & Nakamae, K. (1995). Elastic-modulus of the crystalline regions of cellulose polymorphs. *Journal of Polymer Science Part B-Polymer Physics*, *33*(11), 1647–1651.
Noh, K. T., Lee, H. Y., Shin, U. S., & Kim, H. W. (2010). Composite nanofiber of bioactive glass nanofiller incorporated poly(lactic acid) for bone regeneration. *Materials Letters*, *64*(7), 802–805.
Ramirez, M. A. (2010). Cellulose nanocrystals reinforced electrospun poly(lactic acid) fibers as potential scaffold for bone tissue engineering. *Department of Wood & Paper Science* (Vol. Master of Science, p. 75). Raleigh: North Carolina State University.
Shi, Q. F., Chen, C., Gao, L., Jiao, L., Xu, H. Y., & Guo, W. H. (2011). Physical and degradation properties of binary or ternary blends composed of poly (lactic acid), thermoplastic starch and GMA grafted POE. *Polymer Degradation and Stability*, *96*(1), 175–182.
Shi, Q. F., Mou, H. Y., Gao, L., Yang, J., & Guo, W. H. (2010). Double-melting behavior of bamboo fiber/talc/poly (lactic acid) composites. *Journal of Polymers and the Environment*, *18*(4), 567–575.
Vankrevelen, D. W. (1975). Some basic aspects of flame resistance of polymeric materials. *Polymer*, *16*(8), 615–620.
Vieira, A. C., Vieira, J. C., Ferra, J. M., Magalhaes, F. D., Guedes, R. M., & Marques, A. T. (2011). Mechanical study of PLA–PCL fibers during in vitro degradation. *Journal of the Mechanical Behavior of Biomedical Materials*, *4*(3), 451–460.
Xiang, C. H., Joo, Y. L., & Frey, M. W. (2009). Nanocomposite fibers electrospun from poly(lactic acid)/cellulose nanocrystals. *Journal of Biobased Materials and Bioenergy*, *3*(2), 147–155.
Yang, F., Murugan, R., Wang, S., & Ramakrishna, S. (2005). Electrospinning of nano/micro scale poly(L-lactic acid) aligned fibers and their potential in neural tissue engineering. *Biomaterials*, *26*(15), 2603–2610.
You, Y., Min, B. M., Lee, S. J., Lee, T. S., & Park, W. H. (2005). In vitro degradation behavior of electrospun polyglycolide, polylactide, and poly(lactide-co-glycolide). *Journal of Applied Polymer Science*, *95*(2), 193–200.
Yue, Y. (2011). A comparative study of cellulose I and II fibers and nanocrystals. *School of Renewable Natural Resources* (Vol. Master of Science, p. 73). Baton Rouge: Louisiana State University.
Zhou, C. J., Wang, Q. W., & Wu, Q. L. (2012). UV-initiated crosslinking of electrospun poly(ethylene oxide) nanofibers with pentaerythritol triacrylate: Effect of irradiation time and incorporated cellulose nanocrystals. *Carbohydrate Polymers*, *87*(2), 1779–1786.
Zhou, C. J., Chu, R., Wu, R., & Wu, Q. L. (2011). Electrospun polyethylene oxide/cellulose nanocrystal composite nanofibrous mats with homogeneous and heterogeneous microstructures. *Biomacromolecules*, *12*(7), 2617–2625.
Zhou, C. J., & Wu, Q. L. (2011). A novel polyacrylamide nanocomposite hydrogel reinforced with natural chitosan nanofibers. *Colloids and Surfaces B-Biointerfaces*, *84*(1), 155–162.
Zhou, C. J., Wu, Q. L., Yue, Y. Y., & Zhang, Q. G. (2011). Application of rod-shaped cellulose nanocrystals in polyacrylamide hydrogels. *Journal of Colloid and Interface Science*, *353*(1), 116–123.
Zhou, C. J., Wu, Q. L., & Zhang, Q. G. (2011). Dynamic rheology studies of in situ polymerization process of polyacrylamide–cellulose nanocrystal composite hydrogels. *Colloid and Polymer Science*, *289*(3), 247–255.
Zong, X. H., Kim, K., Fang, D. F., Ran, S. F., Hsiao, B. S., & Chu, B. (2002). Structure and process relationship of electrospun bioabsorbable nanofiber membranes. *Polymer*, *43*(16), 4403–4412.